FILE

INTERNAL DOCUMENT 192

I.O.S.

Pop-up Pore Pressure Instrument

PUPPI II Development

Penetration Calculations & Hydrodynamics

A.R. Packwood

October 1983

Internal Document No. 192

NATURAL ENVIRONMENT RESEARCH COUNCIL

INSTITUTE OF OCEANOGRAPHIC SCIENCES

INSTITUTE OF OCEANOGRAPHIC SCIENCES

Wormley, Godalming,
Surrey GU8 5UB
(042-879-4141)

(Director: Dr. A. S. Laughton, FRS)

Bidston Observatory,
Birkenhead,
Merseyside L43 7RA
(051-653-8633)
(Assistant Director: Dr. D. E. Cartwright)

Crossway,
Taunton,
Somerset TA1 2DW
(0823-86211)
(Assistant Director: M. J. Tucker)

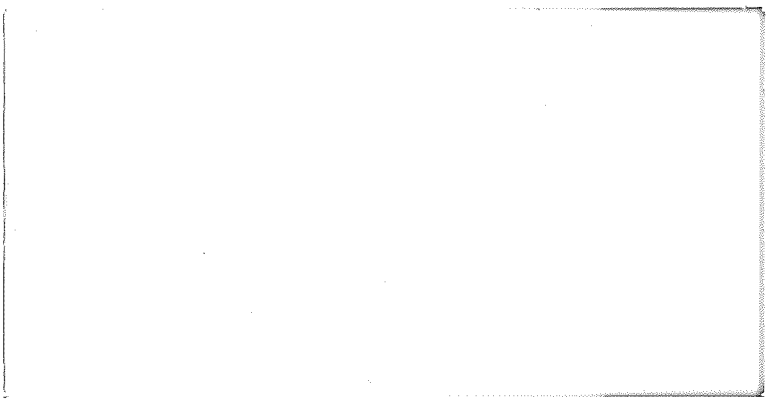

Pop-up Pore Pressure Instrument

PUPPI II Development

Penetration Calculations & Hydrodynamics

A.R. Packwood

October 1983

Internal Document No. 192

Institute of Oceanographic Sciences,
Brook Road,
Wormley,
Godalming,
Surrey,
GU8 5UB.

CONTENTS

POP-UP PORE PRESSURE INSTRUMENT

PUPPI II DEVELOPMENT

PENETRATION CALCULATIONS & HYDRODYNAMICS

INTRODUCTION

The configuration of the system was for the most part defined by the specification to measure pore water pressures at 3 m depth in the sediment and that it should be a free-fall derivative of the ill-fated Puppi I. This demanded that the instrument be composed of a 3 m disposable probe and ballast weights, release gear, instrumentation, logger, command pinger and buoyancy, all capable of withstanding 5000 m water pressure. These were to be suitably arranged to ensure a clear window to the surface for the command pinger, a strong righting moment to correct any perturbations to the fall angle on descent, a clean separation on release and a reasonable free-fall velocity. Hence the instrument quickly evolved to the form shown in fig. 1.

PENETRATION

The free-fall momentum had to be sufficient to push the probe into the sediment. The weight plate should then brake the fall and prevent the instrument from being buried in the mud. The main question to be answered was what ballast weight and terminal velocity would be necessary to accomplish this in deep ocean sediments. To examine instrument penetration the mathematical model reviewed by Ove Arup Partners (1982), with certain corrections discussed in Appendix A, was employed. The resistance to partial embedment for three stage entry can be written in the form

$$\left.\begin{aligned}
&\text{cone entry} \quad F_1 = A.N_{cd}.C_u(Z).\left(\frac{Z}{H}\right)^2 \quad \ldots . Z < H \\
&\text{shaft entry} \quad F_2 = A.(N_{cd}.C_u(Z) + p_s.g.\bar{Z}) + \pi.D.\bar{Z}.x_d.C_u\left(\frac{\bar{Z}}{Z}\right) \quad \ldots . H < Z < L+H \\
&\text{plate entry} \quad F_3 = A.(N_{cd}.C_u(Z) + p_s.g.\bar{Z}) + \pi.D.L.x_d C_u(\bar{Z} - \frac{L}{2}) \\
&\qquad + A_1\,(N_{cd}.C_u(Z') + p_s.g.Z') + \pi.D_1.Z'.x_d.C_u\left(\frac{Z'}{2}\right) \quad \ldots . Z > L + H
\end{aligned}\right\} \quad (1)$$

where $A = \frac{\pi D^2}{4}$, $A_1 = \frac{\pi}{4}(D_1^2 - D^2)$, p_s = sediment density

$C_u(Z) = a + b.Z$ = sediment shear stress profile

$\bar{Z} = Z - H$, $Z' = Z - H - L$

x_d = dynamic shaft adhesion factor, assumed constant

N_{cd} = dynamic end-bearing capacity factor, assumed constant,

see fig. 2 for other dimensions.

The equation for free-fall impact at the sea-floor is then

$$m_e \ddot{Z} = W_{nett} - k\dot{Z}^2 - F(Z) \qquad (2)$$

Here m_e is the effective mass of the instrument, including added mass, W_{nett} is its nett weight in water, $k\dot{Z}^2$ is the instrument drag in water ($k = \frac{1}{2}\rho SC_D$) and F(Z) takes the form of $F_{1,2,3}$ from (1) dependent on the value of Z. The values of the various coefficients in (1) have been obtained empirically for several different sediment types and are given in the report by Ove Arup Partners (1982). The values of x_d and N_{cd} are functions of $\dot{Z}$ but it was found that in this problem the variation was small so averaged values were taken such that $N_{cd} = 14$ and $x_d = 1.2$. The sediment density ρ_s was taken to be 1600 kg/m³. A range of values of a and b were investigated to simulate various shear strength profiles. It is realised that the equations (1) do not represent a particularly good or realistic model of soil failure and resistance to penetration but for the engineering purposes in hand this crude empirical approach is probably justifiable.

Prior to the trials values of m_e, k and W_{nett} could only be estimated. W_{nett} and k were later found to be within 5% but m_e was 30% too low. This is discussed in the following section. The instrument drag was estimated from known drag coefficients for a cylinder on end and for the Benthos spheres in ribbed hard hats which together gave $k \simeq 300$ kg/m. The effective mass was based on known component weights in air with ad hoc estimates of entrained water mass from some theoretical calculations, e.g. see Newman (1977), this gave $m_e \simeq 320 + B_a$ (kg) uncorrected, where

B_a = weight of lead ballast in air.

The nett weight in water was estimated at $W_{nett} = (22 + 0.91\ B_a)\ .\ g(N)$ where $g = 9.81\ m/s^2$. This gave free-fall terminal velocities in the range 1.5 to 2.5 m/s for a suitable range of values of B_a.

The geometric values used in (1) were D = 5 cm, H = 10 cm, L = 3.05 m and D_1 = 30 cm, see fig. 2. Knowing all this (2) could be numerically integrated, using standard NAG, Runge-Kutta integration routines, for different values of a, b and B_a, to give the velocity decay and final penetration. Fig. 3 shows velocity penetration curves for various ballast weights in a medium strength sediment $C_u(Z) = 3 + 1.2Z$ kN/m². Fig. 4 indicates how the sediment strength influences penetration of a heavily loaded instrument. The weak sediment has shear strength given by $C_u = 1.5Z$ kN/m² and the stronger one $C_u = 5 + 1.2Z$ kN/m².

Plotting the deceleration curves corresponding to the velocity curves of Fig. 3 indicated that the fitting of a vertically mounted 1g accelerometer would show some useful information and may be capable of measuring the penetration. The calculations clearly indicated that the accelerometer would show when the weight plate entered the mud and it could also give the rest angle of the instrument if this angle were not small. Fig. 5 shows typical calculated deceleration curves for different sediment types and the same instrument weight. The weakness of the mathematical model is demonstrated by the fact that the deceleration does not return to zero when the instrument comes to rest. See Appendix A for a further discussion of this.

It is clear that with a judicious choice of ballast weight the instrument in its chosen configuration could be made to penetrate to a depth of 3 m in all but the strongest deep sea sediments. On the satisfactory basis of these early calculations the instrument then went forward to detail design and manufacture.

From detail engineering drawings the instrument nett weight in water was calculated more accurately to be

$$W_{nett} \simeq 36 + N \times 19 \text{ kg} \qquad (3)$$

where N is the number of lead ballast weights weighing ≃ 21 kg in air. The values of N shown in fig. 3 correspond to that given by (3) for the same nett weight.

The distance required to reach 99% of terminal velocity when dropped from rest is given by

$$S_{99} = \frac{1.95\ m_e}{k} \qquad (4)$$

This result is obtained by direct integration of the free-fall equation of motion and indicates that even the heaviest ballasted instrument will be very close to terminal velocity after having fallen only 4 m.

INSTRUMENT TRIALS

The instrument was dropped in ≃ 20 m of water into a sediment that was thought to be similar to that in the deep sea sites of interest. Previous cores had shown this to be the case (see Schultheiss P.J. et. al. (1983)). It was decided for prudence that the first drop would be made with 6 weights. Divers were in attendance to make observations and assist with the instrument recovery. A summary table of the trials data is shown in Table 1. The pore pressure results are discussed in Schultheiss P.J. et. al. (1983). Unfortunately the accelerometer electronics did not work on every drop but 5 records were obtained. The divers made what observations they could during descent and ascent but accurate fall

and rise times were difficult to make because of poor visibility.

The acceleration record was held in EPROM's and dumped to a jet pen recorder for analysis. Typical accelerometer traces are shown in fig. 6. The instrument electronics saturated at the instant of the drop so the peak acceleration is not shown. Theoretically the acceleration curve has the form

$$\ddot{S} = \frac{W_{nett}}{m_e} \operatorname{sech}^2 \left\{ \left(\frac{W_{nett}\, k}{m_e} \right)^{\frac{1}{2}} t \right\} \qquad (5)$$

Integrating the measured free-fall acceleration curve gives the terminal velocity as does integrating the penetration deceleration curve. Double integrating this latter curve should give the penetration. The results of these integrations, generally obtained by using Simpson's rule, are also given in Table 1 along with the steady tilt angle where measurable. The double integration of the penetration curves, integrating bit by bit to get the velocity curve and integrating this to give final penetration, yields penetrations greatly in excess of those measured. This is probably due to the uncertainty of the start of the penetration event. A small error of 0.25 sec when the instrument is travelling at 2 m/s or more results in a large error in the final penetration.

The one incident clearly defined on the penetration curve is the penetration of the weight plate. The area under the weight plate penetration curve may be integrated and converted to a constant deceleration over a time interval defined by the mid-point of the rise and fall slopes of the curve, see sketch.

The penetration of the weight plate can then be determined with improved accuracy from

$$Z_p = u_p \Delta t - \tfrac{1}{2} f (\Delta t)^2 \qquad (6)$$

where u_p = area under curve (shaded) and $f = u_p/\Delta t$. This simple approximate method overcomes the errors involved in a double integration and gave penetration to within an inch or so. Such accuracy is rather poor when the total plate penetration may only be 2 - 3 in, but it gave better results than the double integration method which again over estimated the penetration by a considerable amount, even over this limited range.

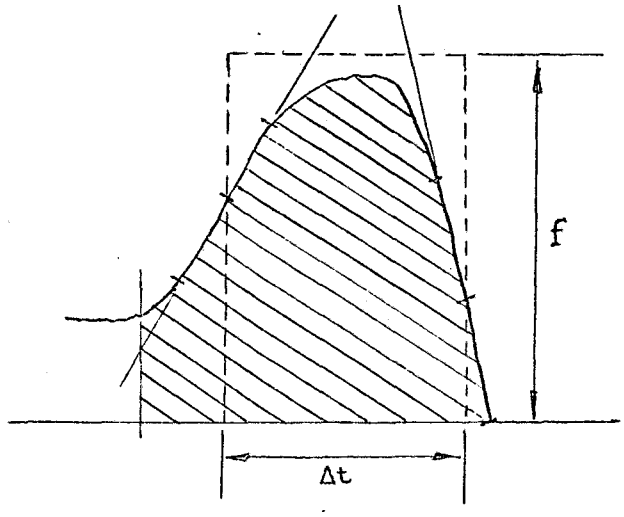

From the tabulated results, integrations giving penetration were not very good unless the weight plate entered the sediment. Integrations giving velocity also varied according to whether the drop was integrated or the penetration. Penetration integration gave lower terminal velocities than the drop in the two cases where this comparison was made. It was the case that where the final rest angle was appreciable, the integrated accelerometer trace gave terminal velocities lower than expected. Since the accelerometer was not gimballed or fixed to a stabilized platform, it could not give the true deceleration record when the instrument was tilted. The drop curve can be integrated with greater confidence since generally the instrument was observed to descend at only small angles but unfortunately the peak acceleration was missing because of the amplifier saturation problems. It is possible to fit the tails of these curves using (5) and predict the peak value. Increasing k steepens the curve and changing m_e, knowing W_{nett}, changes the peak value. After some trial it was found that k ≃ 300 kg/m and m_e given by

$$m_e = 520 + 21N \text{ (kg)} \qquad (7)$$

gave good fits to the curves for 4 and 8 weights. This value of m_e is ≃ 200 kg more than that previously estimated whereas k is as predicted. Much more water was apparently carried with the instrument, presumably around the ribbed hard hats of the spheres and in their wake, than simple theoretical calculation had predicted. This important result influences the calculated velocity - penetration curves of fig. 3. The corrected curves with m_e given by (7) and W_{nett} given by (3) are shown dashed on fig 3. The penetrations are increased by 0 (20 cm) in most cases, and the deceleration is ∿ 10% lower initially. This partially explains why the initial penetration event was not easily detected by the accelerometer.

The most important observation from the trials was that on 5 of the 10 drops penetration angles in excess of 10^o were reported by the divers. The limited measuring accuracy from the jet pen recorder trace of the accelerometer record generally gave angles several degrees smaller than measured. This may have been due to the insensitivity of the instrument at small tilt angles which has a cosine response such that

$$\phi = \cos^{-1} \left(1 - \frac{\Delta g}{g}\right) \qquad (8)$$

where Δg is the measured residual acceleration and g is the acceleration due to gravity. Measurement accuracy from the recorder trace was ±.07 m/s² which is equivalent to ± 7^o at small angles improving to ± 1^o at ∿ 20^o.

It was thought that since the instrument came to rest at an angle it must have had some initial angle before entering the sediment. The increased drag

on the nose of the probe entering at an angle would induce a turning moment on the instrument tending to increase the pitch angle. Hence any quite small angle of pitch that the instrument assumed in the water would be magnified upon penetration. The hydro-dynamic stability of the instrument appears to be crucial in this respect, and from operational and instrument survivability considerations the device must be made to free-fall stably at zero pitch angle.

PUPPI STABILITY IN FREE-FALL

To model the free-fall pitch stability it was necessary to assume a mass distribution in order to find the pitch axis of the instrument. The assumed distribution of added mass was somewhat arbitrary. Most was lumped around the spheres and smaller amounts of entrained water mass distributed at the major mass centres as shown in fig. 7 for the 8 weight configuration. The mass distribution was balanced by taking moments giving $\bar{x}$, the distance of the centre of pitch from the horizontal centre line of the two spheres. The moment of intertia in pitch was estimated assuming the masses to be point masses. The static pitch righting moment M_o due to the weights in water of the ballast and probe and the buoyancy of the spheres is given approximately for small pitch angles by

$$M_o = (W_p\ (2.6 - \bar{x}) + W_b\ (1 - \bar{x}) + B\bar{x})\ \phi \quad \text{Nm} \qquad (9)$$

where W_p = probe weight in water = 265 N

W_b = ballast weight in water

B = nett buoyancy of spheres = 324 N (making some allowance for the weights of the electronics tubes etc.)

and ϕ = pitch angle (radians)

The relevant quantities for the various parameters listed above necessary for the stability calculation are given in the table on fig. 7 for a range of ballast weights.

A tail fin is the obvious method by which the free-fall stability may be improved. The stability of the instrument was therefore investigated with and without a tail in an attempt to optimise the instrument response assuming at some time t = 0 that it was at some initial angle ϕ_o.

Assume the instrument to be free-falling at its terminal velocity U_T. Observed from a reference frame moving at this velocity the instrument is free to move in pitch and lateral displacement, ignoring spin or any motion out of the plane in which the observations are made. Consider the forces acting on the instrument sketched below. The only de-stabilizing force comes from any

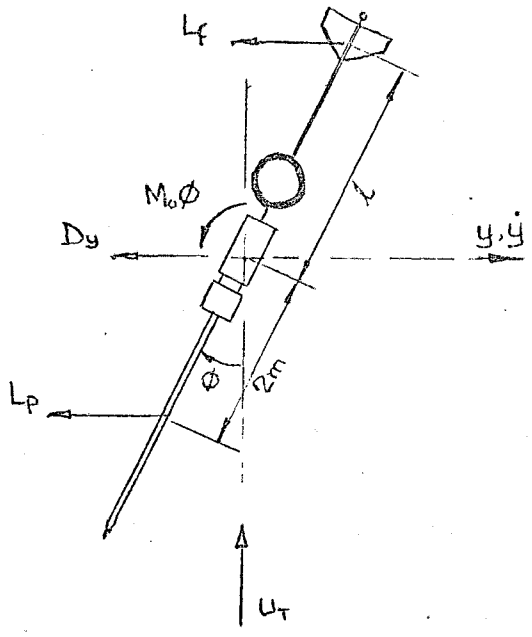

lift force L_p that may be generated on the probe. For ϕ positive L_p and any lift generated at the fin, L_f, act as shown. The force D_y is the lateral drag force which will always act in the direction opposing the lateral velocity $\dot{y}$. For this system the equations of motion become

$$M_e \ddot{y} = - L_f - L_p - D_y \tag{10}$$

$$I\ddot{\phi} = - M_o\phi + 2L_p - \ell L_f \tag{11}$$

The fin lift is given by

$$L_f = q\, S_f\, a_f\, \alpha \tag{12}$$

where $q = \frac{1}{2}\rho\, u_T^2$, S_f = fin area, a_f is the fin lift curve slope $\simeq \pi$ for low aspect ratio flat plate fins and α is the relative free-stream angle of incidence of the flow on the moving fin. Assuming small angles and that linearizations can be made

$$\alpha \simeq \phi + \frac{1}{u_T}(\dot{y} + \ell\dot{\phi}) \tag{13}$$

For the probe lift it is assumed that the lift on the pitched cylinder may be linearized to a similar form

$$L_p = q\, S_p\, a_p\, \alpha' \tag{14}$$

where $\alpha' = \phi + \frac{1}{u_T}(\dot{y} - 2\dot{\phi})$, $S_p \simeq 3 \times .05$ m^2 and $a_p \simeq 1$.

Heorner (1958) suggests that L_p has the non-linear form

$$L_p = q\, S_p \times 1.1 \sin^2 \alpha' \cos \alpha'$$

but for the purposes of our rather crude model eqn. (14) will be used. The lateral drag is simpler and may be written

$$D_y = \tfrac{1}{2}\rho\, (SC_D)_y\, \dot{y}|\dot{y}| \tag{15}$$

where $(SC_D)_y$ is the sum of products of lateral drag coefficients and projected areas of the instrument components which comes to $(SC_D)_y = 1.44 + 1.2\, S_f$ (m^2).

The equations of motion (10) and (11) can be solved numerically with the appropriate substitutions from (13), (14) and (15), once more using standard Runge-Kutta integration routines. Fig. 8 shows the pitch angle response curves for the vehicle with no fins and 3 loading conditions, for large fins on a 2.1 m

tail arm and small fins mounted on the spheres. The curves show that without fins the instrument is underdamped. Large fins on a tail arm extending above the spheres over-damp the system and the time to reach near steady-state is not much improved. To obtain near critical damping small fins could be attached outboard of the spheres and electronics tubes. There are a number of advantages associated with this latter solution.

i) The time to get back to steady state following a perturbation is minimized.

ii) The fins are in an exposed position and therefore may be expected to function well hydrodynamically i.e. they are not shielded or in the turbulent wake of upstream instrument components.

iii) The fins may be located so as to induce no unstable turning moments when the instrumentation and buoyancy separates from the probe and ascends to the surface.

iv) There is negligible additional weight penalty in this solution. This is a consideration since there is only an estimated 17.7 kg excess buoyancy to bring the recoverable parts back to the surface.

An additional way of increasing the righting moment would be to fill the hollow probe with lead. Approximately 42 kg of lead ballast could be used in this way reducing the number of weights carried on the weight plate by two. This moves the pitch centre lower and increases the pitch inertia considerably. The static righting moment is increased by ≃ 27%. The details are given in the table on fig. 7. Using these figures in the stability analysis assuming the instrument is fitted with small fins mounted on the spheres gives the pitch response shown dotted on the lower figure in fig. 8. The faster response causes the instrument to overshoot further but after 5 sec the response is almost completely damped. Increasing the fin size slightly will reduce this overshoot and further improve the response. Calculations indicate that to reduce the overshoot to 10% of ϕ_o i.e. ≃ 1.2^o the fin area S_f should be increased to 0.2 m^2. The lateral excursion the instrument makes during these oscillations is only about 25 cm from its position at t = 0. Sketches of the fin sizes and their attachment to the spheres are shown in fig. 9. Fins of the dimensions indicated by the shaded area should be fitted at the same height on the two electronics tubes to form a cruciform.

CONCLUDING REMARKS

The instrument trials proved that probe penetration was not a difficulty and that the weight plate does provide adequate breaking to prevent over-penetration. The accelerometer did provide some useful information. In particular it allowed the added mass of the instrument to be more accurately estimated. Penetration however could not be accurately calculated by integrating the accelerometer trace. This may be improved when the vehicle stability is improved so that the probe does not enter the mud at an angle which results in unknown acceleration offsets during penetration. As a tilt angle indicator the accelerometer as presently mounted has poor accuracy at small angles. However the accelerometer trace does clearly indicate whether the weight plate enters the sediment and crude integration of this stronger deceleration does give some measure of the weight plate penetration.

As a result of the tests the instrument stability was brought into question since quite large tilt angles were measured after penetration. Subsequent analysis has shown that the instrument is stable but, as tested, under-damped. It seems that had the drop been much deeper, say 100 m, the instrument may have come to a stable vertical flight-path before entering the sediment. The instrument can be made critically damped by the addition of 4 small fins in a cruciform at the level of the spheres and electronics tubes. If located as shown in fig. 9 the fins should not have any adverse effect on the instrument ascent.

The probe may be lead filled to increase the righting moment if the instrument is perturbed from its vertical path but this would require the fitting of slightly larger fins to regain critical damping. The instrument appears to have sufficient stability so as not to necessitate that it be made to spin in order to maintain a vertical track.

REFERENCES

Hoerner S.F. (1958) Fluid Dynamic Drag
pub. by author

Newman J.N. (1977) Marine Hydrodynamics
pub. M.I.T. press. pp. 402

Ove Arup Partners (1982) Ocean Disposal of Radio-active Waste
D.O.E. Report No. DOE/RW/82.055 March 1982

Schultheiss P.J. et. al. (1983) An instrument to measure differential pore pressures in deep ocean sediments: Pop-Up-Pore-Pressure-Instrument (PUPPI) I.O.S. Report (to appear)

NOTE The penetration equations (1) and (2) are numerically integrated in the program contained in file ARP/PENETROM. The instrument stability equations (10) and (11) are similarly integrated in ARP/ACCLN on the NERC Honeywell computer.

Table 1

Drop #	# Weights	Probe	Accln trace	Measured by divers			Calculated from acceleration traces						
				Tilt Angle (deg)	Penetr'tn (in) from plate	Descent time (sec)	Tilt Angle (deg)	Penetration (in) from plate Z'		Terminal velocity (m/s) U_T			Velocity @ plate entry (m/s)
				ϕ	Z'		ϕ	Double int'gn	Int'gn of plate penetr'tn	Int'gn of drop curve	Int'gn of penetr'tn curve	Theoretical	
1	6	S	✓	5	$1\frac{1}{2} \rightarrow 2\frac{1}{2}$	-	0	8	2	-	1.86	2.2	0.79
2	6	S		0	$2\frac{1}{2}$	-	-	-	-	-	-	-	-
3	5	S		10	$2\frac{1}{2}$	9	-	-	-	-	-	-	-
4	4	L		15	$-1\frac{1}{2}$	-	-	-	-	-	-	-	-
5	7	L		14	2	-	-	-	-	-	-	-	-
6	6	L	✓	0	$2\frac{1}{2}$	8.5	0	45	3	-	2.19	2.2	1.03
7	4	S	✓	25	-12	-	17→18	18	-	2	1.33	2.0	-
8	7	S		6	$3\frac{1}{2}$	-	-	-	-	-	-	-	-
9	8	S	✓	18	$3\frac{3}{4}$	-	16	-	$3\frac{3}{4}$	2 2.4 ext	1.13	2.5	1.13
10	7	S	✓	19	$1\frac{1}{4}$	-	17	16	$2\frac{1}{2}$	-	1.75	2.3	0.73

S = short conical probe

L = long slender probe

ext = extrapolated

Appendix A

A criticism of the partial embedment mechanics contained in the Ove Arup report: Ocean Disposal of Radioactive Waste, March 1982. DOE Report No. DOE/RW/82.055

The criticism starts with the mathematics on page 20 of the above report. Certain errors on this page came to light when the equations were used to model PUPPI partial embedment.

The most serious error is contained in the first line. It is wrong to neglect drag forces. These forces are not small, in fact at the moment of impact they are equal to the term w', the buoyant weight, which is included in equation (6.10). Ignoring drag means the penetrometer accelerates into the sediment as if it were falling in air. This results in an over prediction of the final penetration depth. To be fair to the author, this point is commented on in a later report: "Ocean Disposal of High Level Radio-active Waste" August 82, DOE Report DOE/RW/82.102, section 4.4. Had the equations of motion been integrated numerically, the neglected drag term could have been included quite easily.

The next error occurs in the following equation (6.11a) which describes the reaction to the cone penetration. To start with this approximation is dimensionally incorrect i.e. the term $A_1 Z$ does not have the units of force. Since the cone sectional area increases as Z^2 a better model would be

$$F(Z) = A_1 \left(\frac{Z}{H}\right)^2 \qquad 0 < Z < H$$

this is still an approximation as it ignores terms $O(Z^3)$ and hence is only appropriate if H and thus Z are small compared with say L, the length of the penetrometer.

In equation (6.11a) Z seems to be measured from the tip of the cone to the sediment interface. In (6.11b) it appears Z is measured from the base of the cone to the sediment interface. This may be a reasonable approximation if $H \ll L$ but the notation remains inconsistent. A corrected version of this equation not making the assumption that $Z \simeq \bar{Z}$ would be

$$F(Z) = \left[A_1 + \frac{\pi D^2}{4} N_{cd}\, bH\right] + B_1 \bar{Z} + C_1 \bar{Z}^2, \quad 0 < \bar{Z} < (L-H)$$

These errors mean that the integrated equation (6.12), at the bottom of the page, is also in error. For consistent notation A_1 in (6.12) should be replaced by the terms in square brackets in the equation above. There are several more errors in the expression for $(U_H)^2$. In the second term on the RHS the author appears to have assumed that the penetrometer weight in water is equal to its weight in air and the last term is incorrect even using the erroneous expression for F(Z) in (6.11a) as quoted. The corrected equation for U_H including the correction to (6.11a) should read

$$(U_H)^2 = (U_o)^2 + \frac{2w'H}{M} - \frac{2A_1 H}{3M}$$

These errors follow over to equation (6.13).

It is unlikely that any of these errors will have a very large effect on the final calculated penetration depth of the penetrometers $H \ll L$. Neglecting drag only influences the partial embedment problem i.e. while $Z < L$. Since final penetration is several times L this large initial error may only give a small reduction in final penetration. These conclusions of course do not apply to devices like corers or instruments that are only partially embedded. Great care should therefore be exercised when trying to interpret these results with other penetrometer instruments in mind where the errors could be quite

considerable. Note that these errors have not been corrected in the more recent report DOE/RW/82.102.

General Comments

The Ove Arup model, based on that of Dayal et al. (1980) uses constant values of N_{cd} and α_d throughout the penetration event (N_{cd} = dynamic end-bearing capacity factor, α_d = dynamic shaft adhesion factor). Figs 6.2 and 6.3 of the report show that both vary with penetration velocity. By allowing these parameters to vary using empirical equations to fit the experimental results, a more realistic model could be obtained. It is clear from initial calculations that holding N_{cd} and α_d constant tends to give an underestimate of the penetration depth.

By neglecting fluid drag and N_{cd}, α_d variation with velocity, the Ove Arup equation of motion can be described more generally by

$$M\ddot{Z} = f(Z, Z^2)$$

This has the same form as that describing a non-linear spring with no damping. The equation therefore suggests that as the penetrometer penetrates it puts compression energy into the sediment which is not dissipated and hence after reaching maximum penetration the projectile is accelerated back up the hole and out into the water once more. This hopefully is an unrealistic situation, but it does serve to suggest how poor our understanding is of dynamic soil mechanics. It is clear that only large scale trials will give credance to any of these predictions.

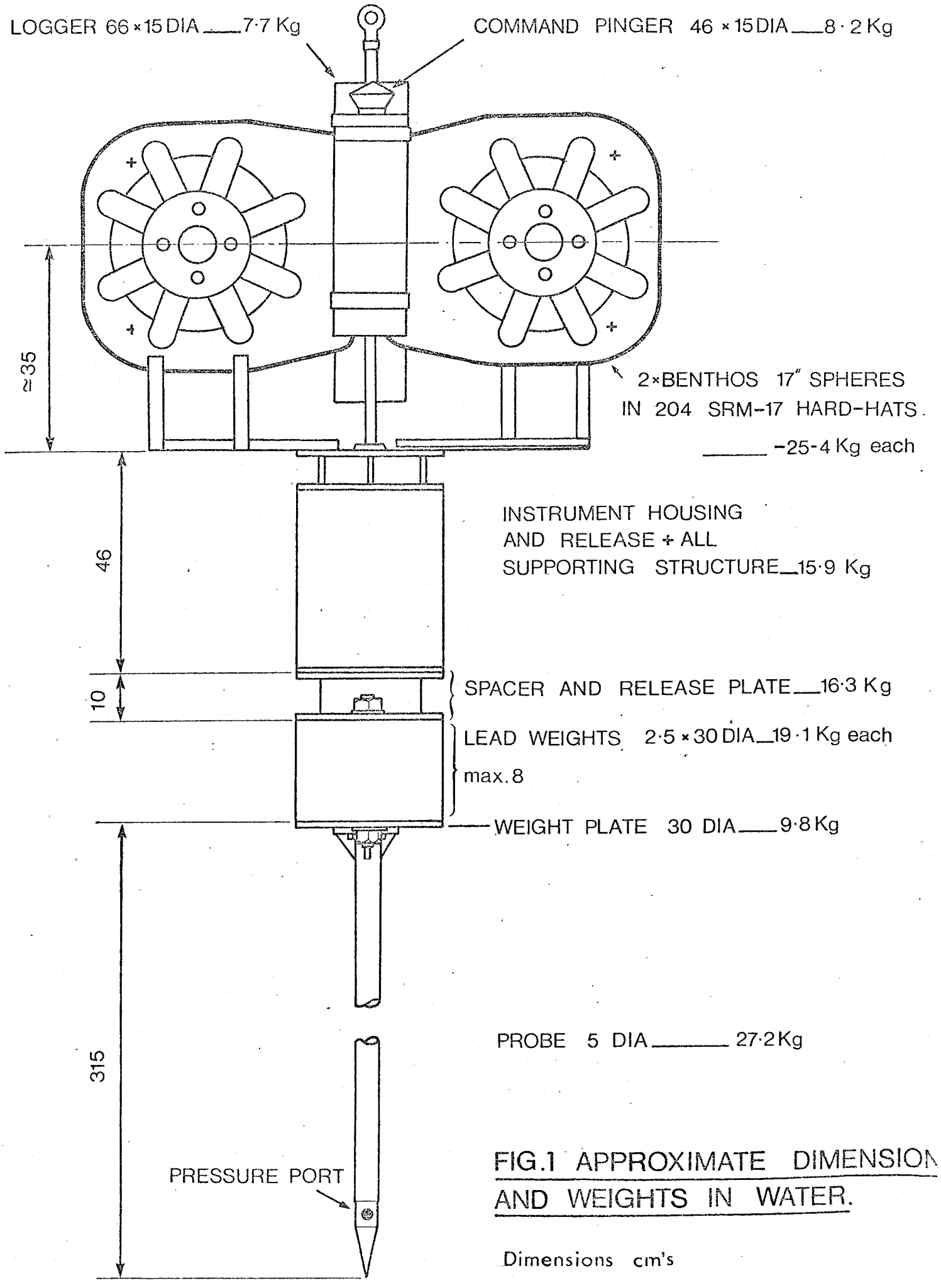

FIG.1 APPROXIMATE DIMENSION AND WEIGHTS IN WATER.

Dimensions cm's

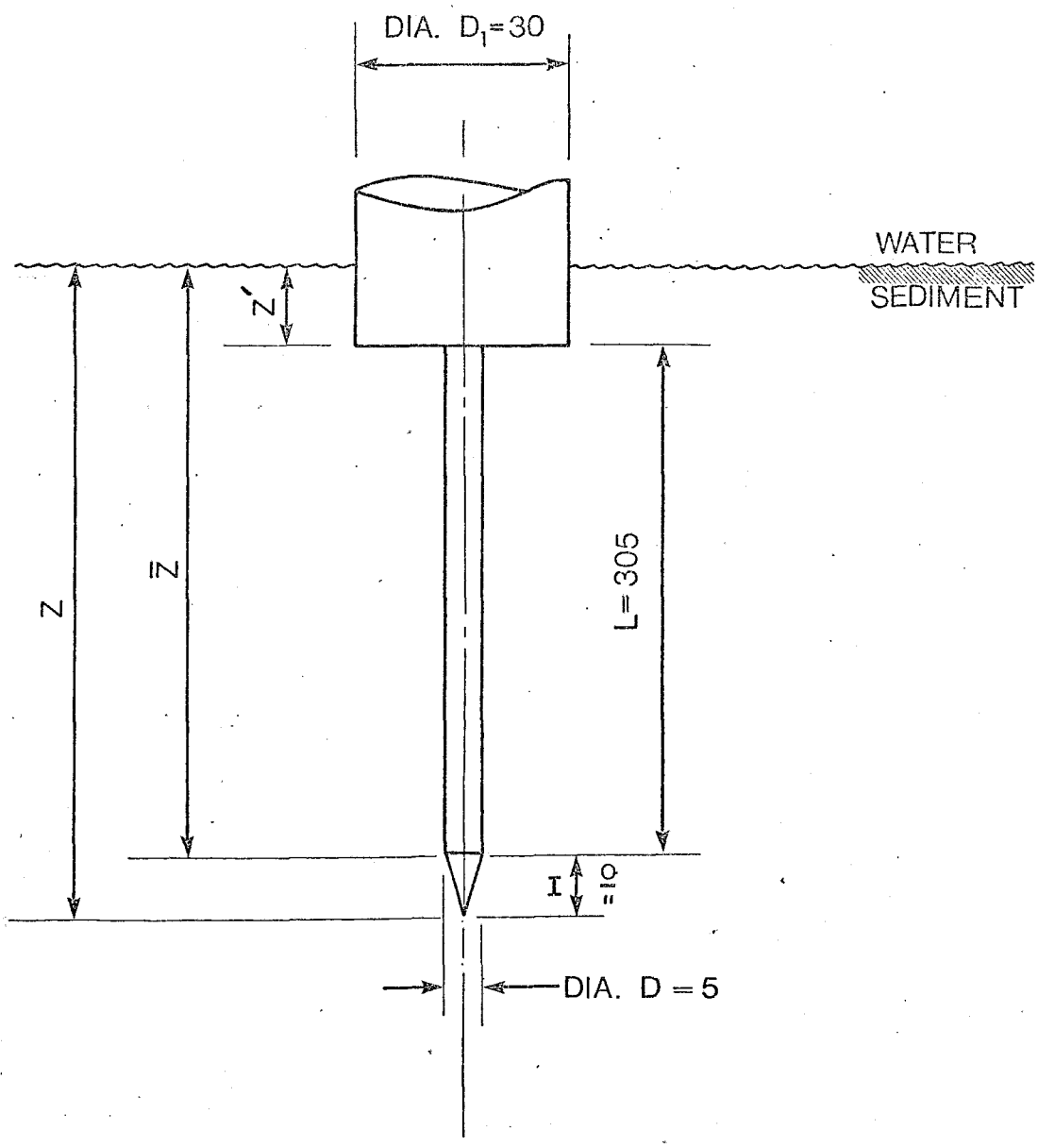

FIG. 2 PENETRATION CO-ORDINATES
DIMENIONS IN CM'S.

Fig. 3 Velocity ~ penetration curves for a range of ballast loadings for penetration into a medium strength sediment $C_u = 3 + 1{\cdot}2\ Z$. KN/m²

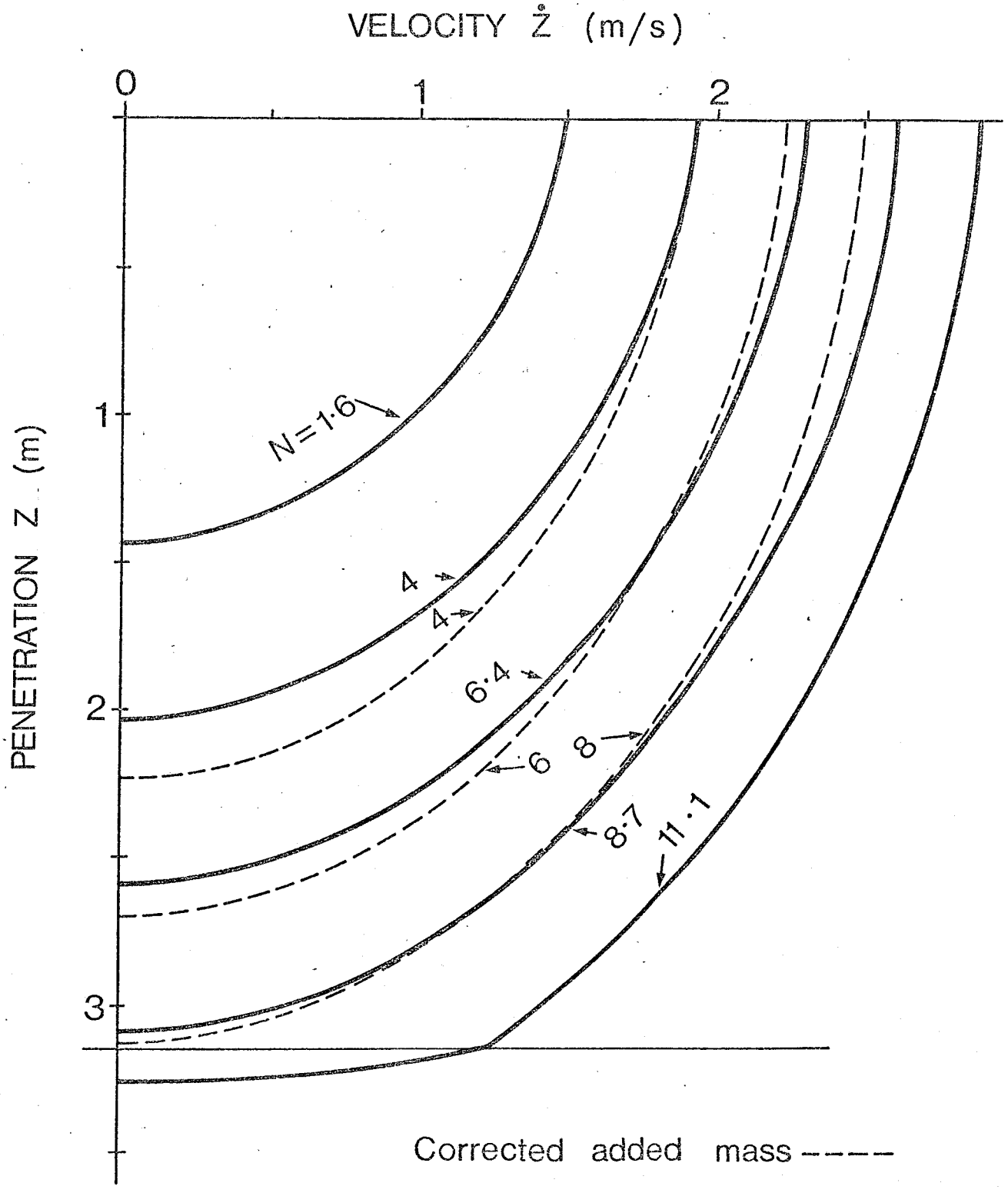

Fig. 4 Velocity~penetration curves for strong and weak sediment types and for an equivelent ballast weight of N = 8·7

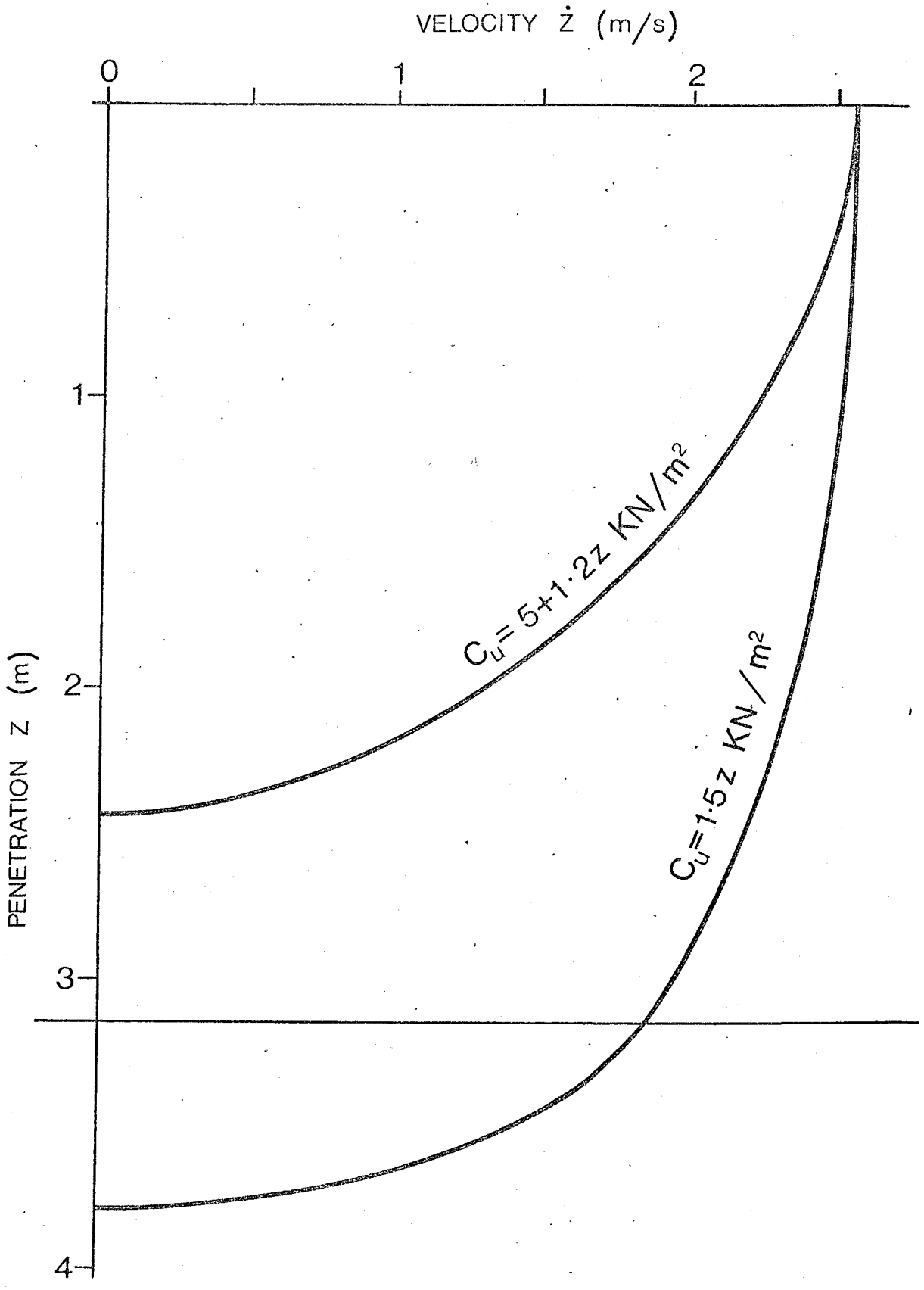

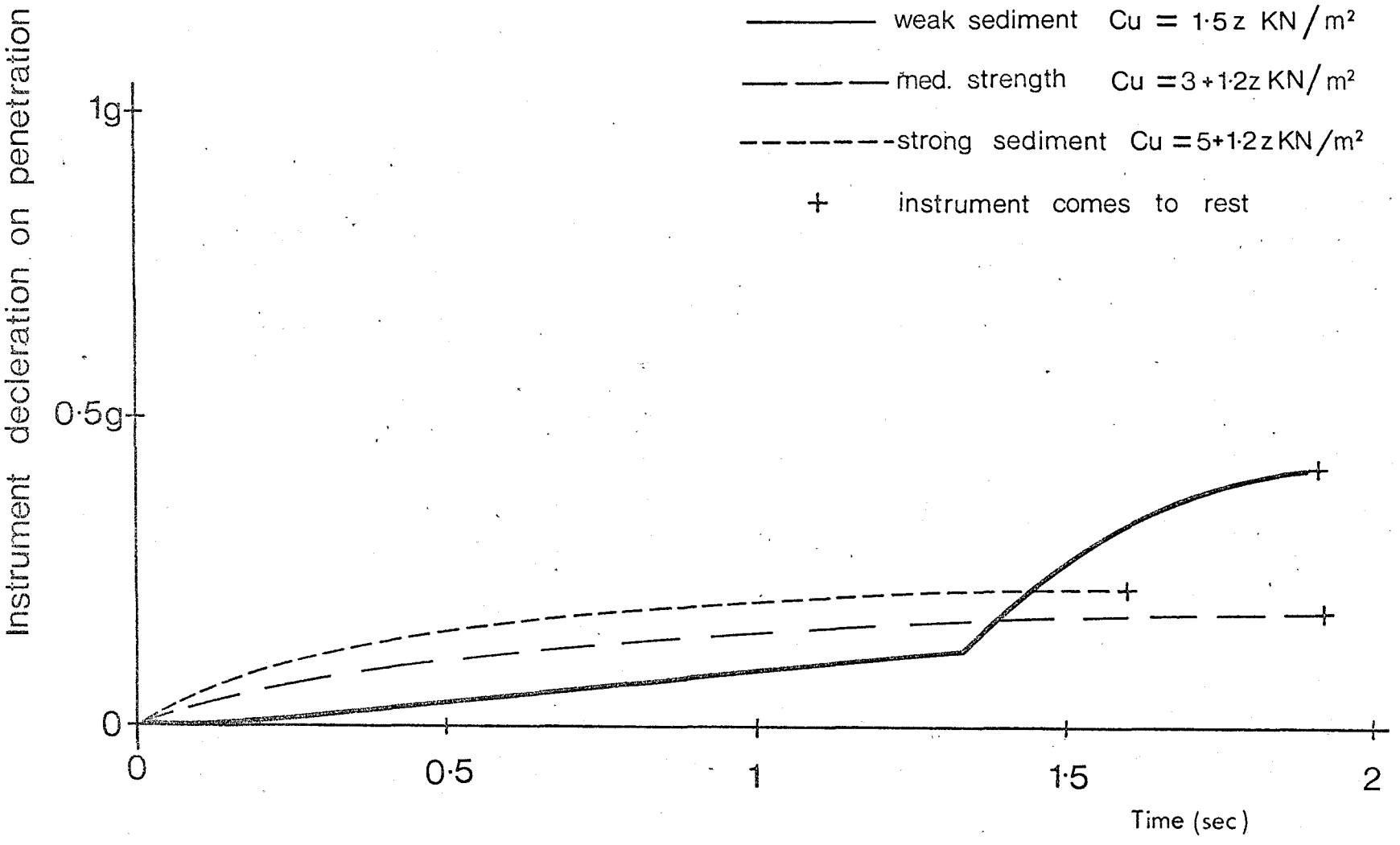

Fig.5 Instrument deceleration curves for various sediment types with ballast equivalent to 8·7 weights. (Note these curves for the uncorrected added mass term)

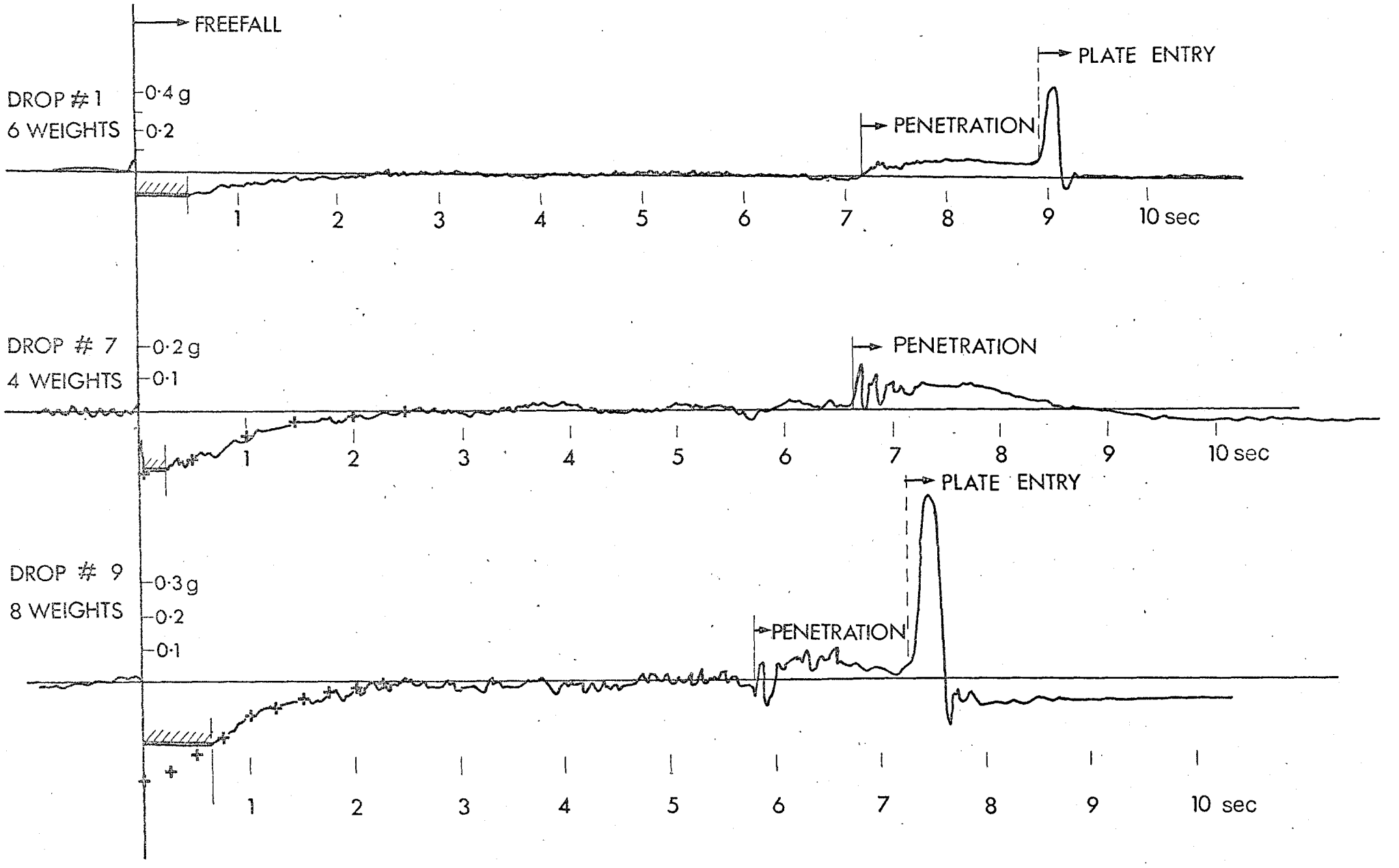

Fig.6 Accelerometer traces from trials with 3 loading configurations

AMPLIFIER SATURATION

\+ FITTED ACCLN. CURVE FROM EQN. (5)

Assumed added mass distribution for configuration with 8 weights Fig. 7

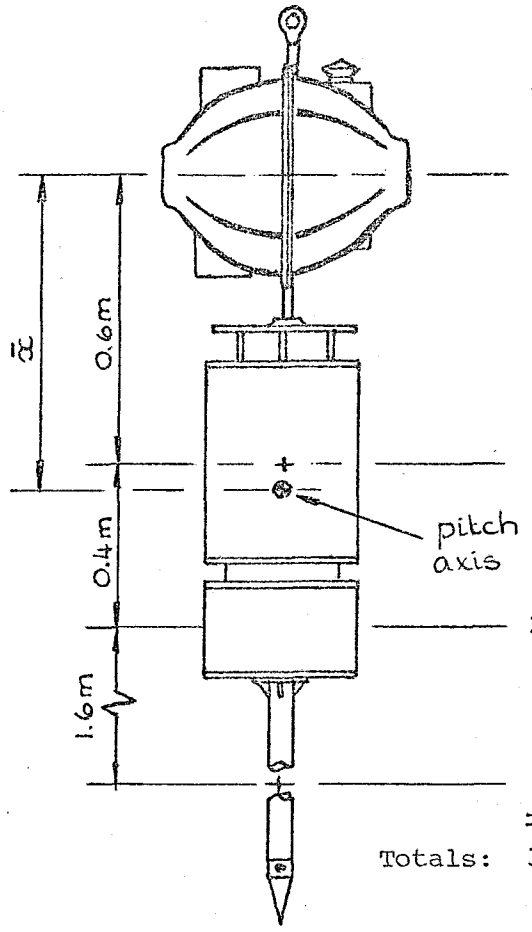

	Mass (kg)	Added mass (kg)	Total (kg)
	80	230	310
	20	80	100
	200	30	230
	30	20	50
Totals:	330	360	690

Instrument parameters for various loading configurations

# Weights	8	6	4	6 + lead filled probe
W_{nett} (kg)	188	150	112	188
U_T (m/s)	2.5	2.2	1.9	2.5
m_e (kg)	690	645	600	690
I (kg.m^2)	344	333	315	486
M_o (Nm)	1430 x ϕ	1260 x ϕ	1077 x ϕ	1814 x ϕ
$\bar{x}$ (m)	0.61	0.57	0.53	0.695

Fig. 8. Instruments response characteristics to an initial pertubation of 11·5° (0·2 rad)

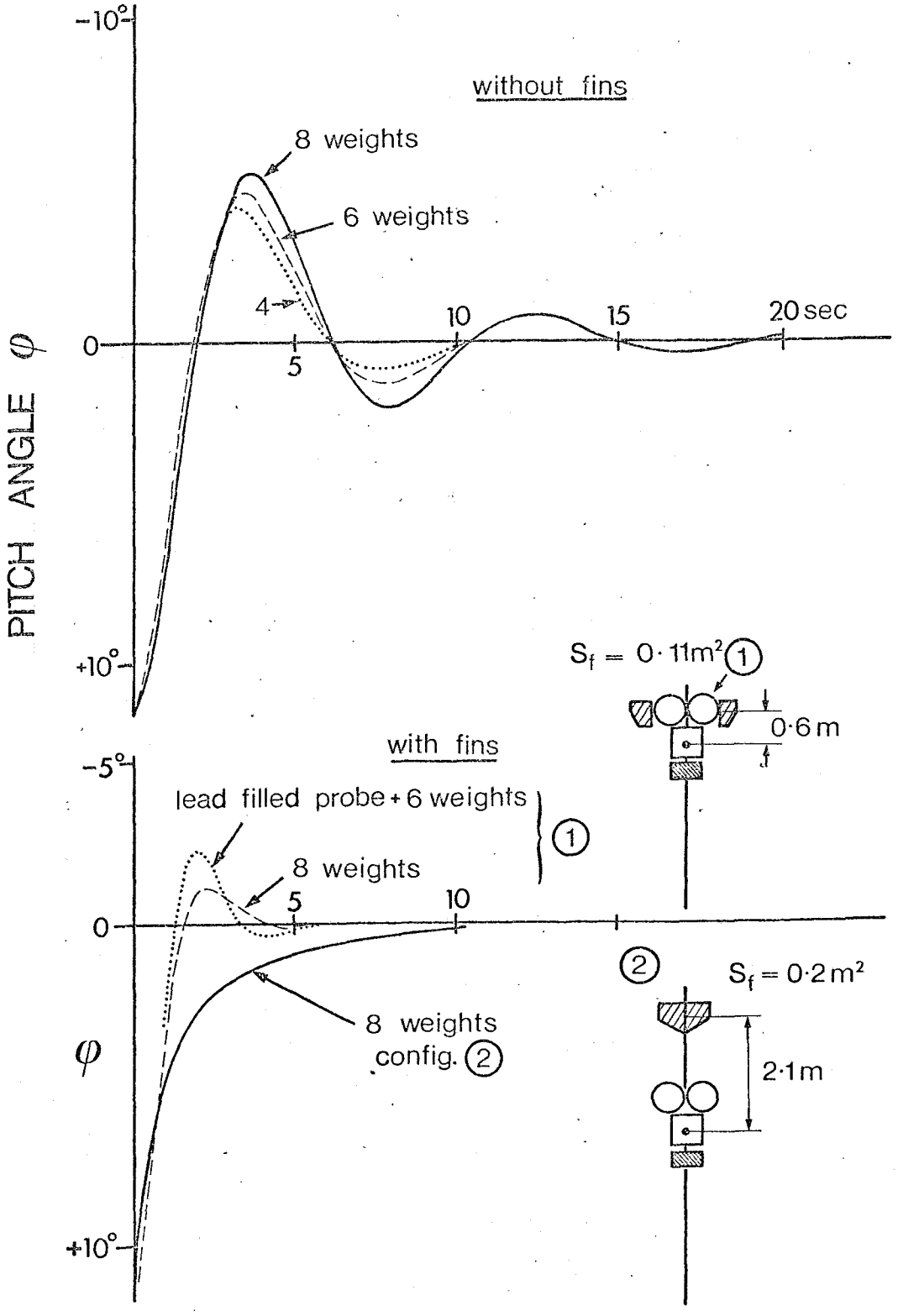

Fig. 9

FIN SIZE FOR PRESENT PUPPI WEIGHT DISTRIBUTION

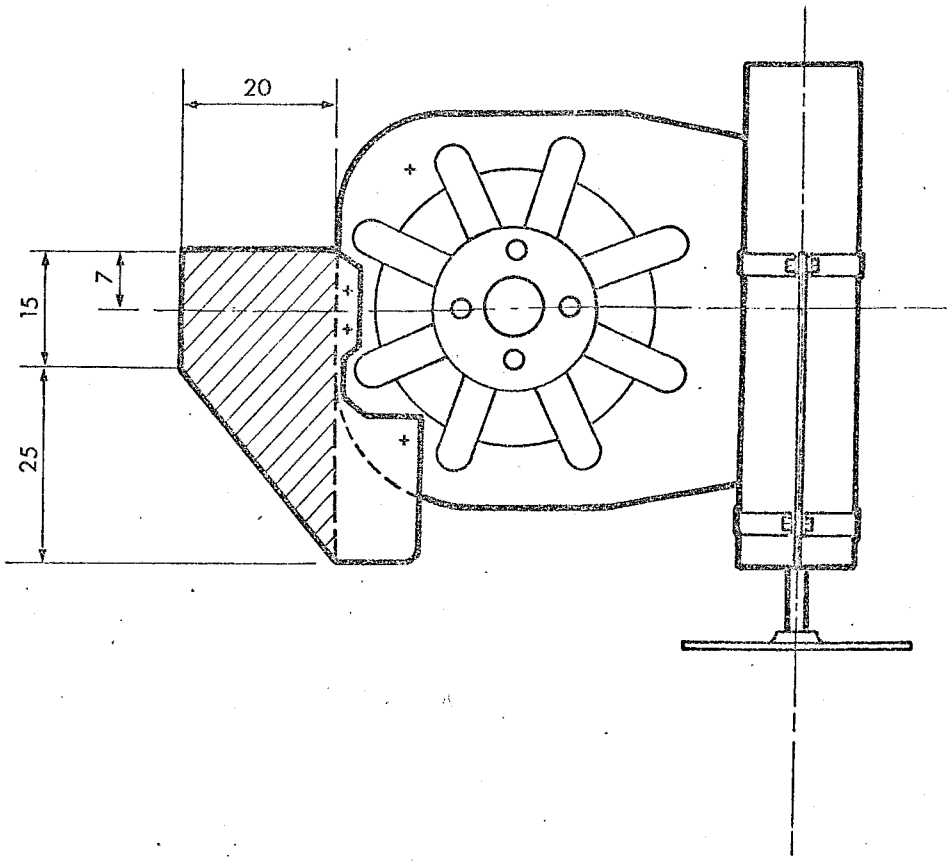

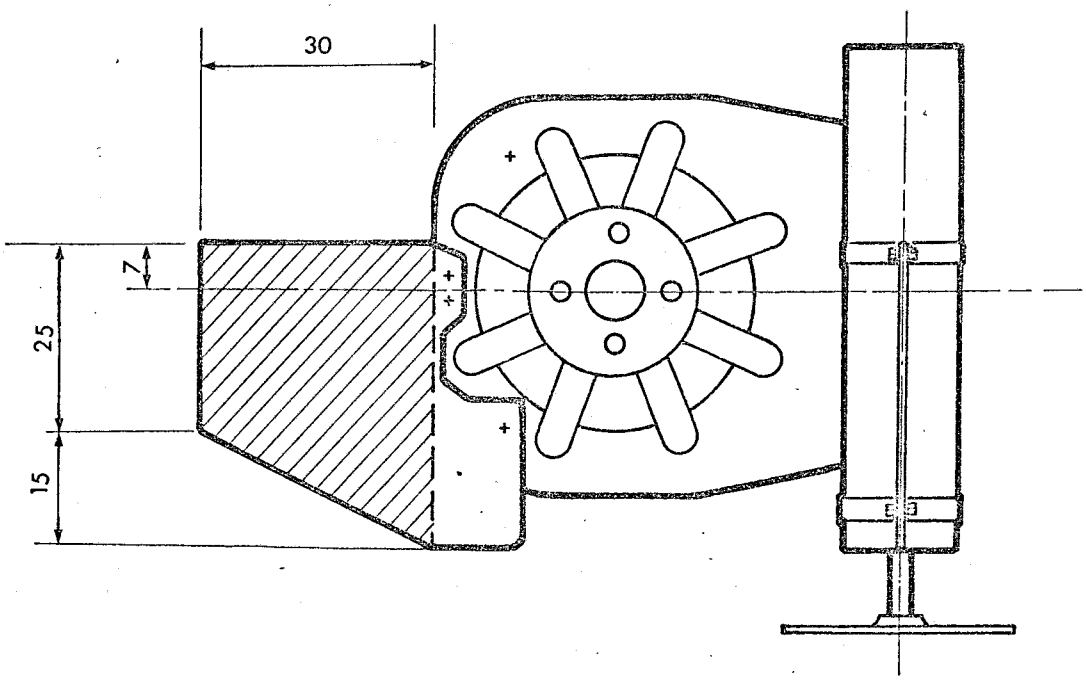

FIN SIZE CRITICAL DAMPING OF THE LEAD-FILLED PROBE VERSION.
DIMENSIONS IN CM'S